2023-01-0053 Published 11 Apr 2023

Enhancing Traffic Safety by Developing Vehicle Safety Envelope with Real Time Data Interface and Machine Learning Based Sensor Fusion Platform

Valentin Soloiu, David Obando Ing, Shaen Mehrzed, Kody Pierce, James Willis, and Aidan Rowell Georgia Southern University

Citation: Soloiu, V., Obando Ing, D., Mehrzed, S., Pierce, K. et al., "Enhancing Traffic Safety by Developing Vehicle Safety Envelope with Real Time Data Interface and Machine Learning Based Sensor Fusion Platform," SAE Technical Paper 2023-01-0053, 2023, doi:10.4271/2023-01-0053.

Received: 08 Nov 2022 Revised: 10 Jan 2023 Accepted: 31 Jan 2023

Abstract

The effectiveness of obstacle avoidance response safety systems such as ADAS, has demonstrated the necessity to optimally integrate and enhance these systems in vehicles in the interest of increasing the road safety of vehicle occupants and pedestrians. Vehicle-pedestrian clearance can be achieved with a model safety envelope based on distance sensors designed to keep a threshold between the ego-vehicle and pedestrians or objects in the traffic environment. More accurate, reliable and robust distance measurements are possible by the implementation of multi-sensor fusion. This work presents the structure of a machine learning based sensor fusion algorithm that can accurately detect a vehicle safety envelope with the use of a HC-SR04 ultrasonic sensor, SF11/C microLiDAR sensor, and a 2D RPLiDAR A3M1 sensor. Sensors for the vehicle safety envelope and ADAS were calibrated for optimal performance and integration with versatile vehicle-sensor platforms. Results for this work include a robust distance sensor fusion algorithm that can correctly sense obstacles from 0.05m to 0.5m on average by 94.33% when trained as individual networks per distance. When the algorithm is trained as a common network of all distances, it can correctly sense obstacles at the same distances on average by 96.95%. Results were measured based on the precision and accuracy of the sensors' outputs by the time of activation of the safety response once a potential collision was detected. From the results of this work the platform has the potential to identify collision scenarios, warning the driver, and taking corrective action based on the coordinate at which the risk has been identified.

Introduction

Relying on human response to unexpected events on the road presents challenges as this response varies as a function of driver age, experience, fatigue and driving scenario conditions (weather, traffic). In fact, a National Highway Traffic Safety Administration (NHTSA) study showed that 94% of crashes are caused by drivers' mistakes caused by factors such as recognition error (driver's inattention, interior and exterior distractions, inadequate surveillance), decision error (driving too fast, taking curves fast, incorrect assumption of other drivers' behavior), performance error (poor directional control, overcompensation), and non-performance error such as driver drowsiness [1]. For this reason, integrating ADAS systems, which enhance the safety in vehicles, is a helpful area of research. Optimized ADAS technologies create a safer driving environment since the reaction time of such safety systems is faster and present a more constant behavior compared to the variable reaction time of humans under different pre-crash and crashing scenarios.

To help mitigate vehicle accidents, novel safety and autonomous technologies have been developed to enhance the safety of drivers and pedestrians worldwide. The adequate integration of distance sensors is fundamental in enhancing safety on the road to further effectively executed autonomous maneuvers. Aside from reducing driving-related fatalities and injuries, autonomous vehicle features have the potential to increase fuel efficiency, reduce traffic congestion and increase traveling speeds [2, 3]. Figure 1 shows red and blue vehicles with integrated distance sensors that have an improper ADAS reaction since they are relying in one sensor signal resulting

TABLE 1 Estimated Distribution of Critical Crash Reasons for Driver Mistakes (Based on 94% of the NMVCCS crashes 2005-2007) [1]

Critical Reason	Number	Percentage
Recognition Error	845,000	41% ± 2.2%
Decision Error	684,000	33% ± 3.7%
Performance Error	210,000	11% ± 2.7%
Non-Performance Error	145,000	7% ± 1.0%
Other	162,000	8% ± 1.9%
Total	2,046,000	100%

FIGURE 1 Vehicle Envelope Integrity through Proper ADAS Reactions from Accurate Sensor Fusion.

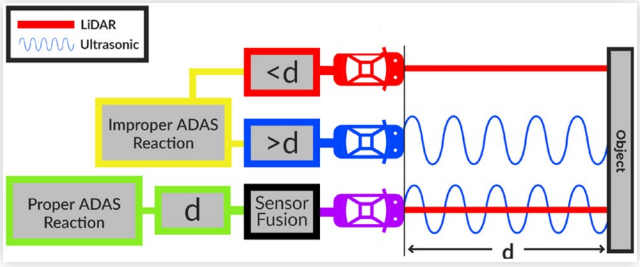

in breaking the safety vehicle envelope. The purple vehicle stays in the vehicle envelope due to integration of multiple signals of sensors making the vehicle safer based on the distance recorded from the target.

At the time of developing ADAS featured vehicles, the selection of integrated sensors and controlling modules substantially affect the production cost. When optimizing an AV research platform with camera, LiDAR, radar, GNSS, and IMU sensors with respect to cost effectiveness and energy efficiency, the total sensor supply costs alone are above $30,000. [4]. Aside from the costs of sensors, there are also substantial costs associated with the integration of an ADAS sensing system. For example, the development of sensor fusion algorithms like the Kalman filter and the subsequent improvements in increased measurement accuracy, reduced measurement noise, and larger measurable ranges are beneficial, but are difficult to develop and are less versatile in practice. However, machine learning alternatives for the Kalman filters improves the versatility and are more easy developed, leading to lower costs.

Vehicle Safety Envelope

When ADAS systems are employed, a safe driving envelope is defined within the vehicle's computer system. This envelope describes a set of boundaries within which the vehicle can be safely operated without losing traction or exceeding the steering, braking, or suspension capabilities [5]. The limits of this envelope is directly related to the maximum capabilities of the tires of the vehicle; these limits are set by the yaw rate and the sideslip [6]. Within this boundary, there always exists a steering input to keep the state of the vehicle within the envelope; however, the vehicle may leave the envelope and still be stable, because the bounds of this envelope are set by steady state assumptions. Empirical testing has shown that the vehicle can leave the envelope and still be stable, and also return to a state within the envelope successfully [7].

Sensors Functioning Principles

The sensors used in this research are HC-SR04 ultrasonic sensor, 2D RPLiDAR sensor and a solid state microLiDAR. All sensors operate on the time-of-flight (ToF) principle. This principle uses the time elapsed after an infrared light is emitted and returns to the receiver to calculate the distance between the emitter and an object. The mathematical

FIGURE 2 ToF Sensor Function

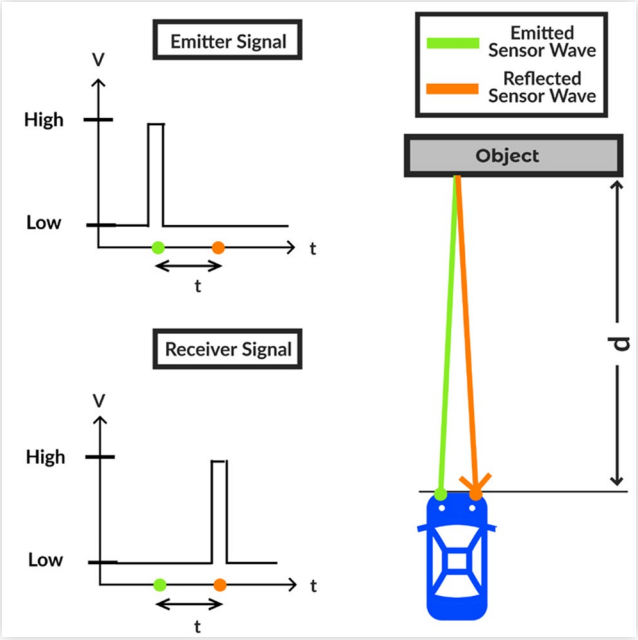

relationship between the wave's velocity v (m/s), time t (s) and distance d (m) to the measured obstacle can be seen below in Eq. 1.

$$d = \frac{vt}{2} \tag{1}$$

The ToF principle used to acquire distance with time and velocity is further visualized in Figure 2. Shown is an emitter pulse signal and a receiver pulse signal after time t. In order to find the distance from an object and emitter, one must consider t being the time needed for an emitted wave to travel to the obstacle then back to the receiver. This is already considered in Eq. 1 as the product of velocity and time is divided by two to find the distance from the sensor to the obstacle.

Ultrasonic Sensors The HC-SR04 sensor emits and receives 40kHz sound wave pulses to determine the ToF with which it can find the distance of an object. This sensor is a widely available and affordable distance sensor used mostly in robotics projects. Similarly functioning but more reliable ultrasonic are used in nearly all parking assisted vehicles. Ultrasonic sensors can generally measure up to 4-5m and therefore be useful in sensor fusion at these relatively short distances.

LiDAR Sensors Light detection and ranging is a technology developed to measure distances and for mapping the environment based on the time of flight principle by using infrared laser pulses. This technology is used because of its accuracy and range. The signal output of this sensor includes X, Y and Z coordinates and intensity values of the point cloud recorded. ToF applied in LiDAR sensors calculates the time it takes for the infrared pulse to travel from the sensor and come back as a reflection of an obstacle in the environment.

The vacuum speed of light, c0, is equal to 299,794,458 m/s, therefore, the ToF equation for LiDAR sensors is as follows [8]:

$$d = \frac{1}{2} c_0 \Delta T \tag{2}$$

Sensor Fusion & Machine Learning

The development of individual sensors involves maximizing measurable ranges and minimizing noise or other constraints. Despite this, sensors will inherently have ideal measurement ranges and physical restrictions. For example, ultrasonic sensors have a shorter accurate measurement range than LiDAR sensors, as the dissipation of ultrasonic sound waves occurs over large distances, whereas infrared light waves used in LiDAR do not dissipate over the same distances. On the other hand, while measuring very short distances, ultrasonic sensors typically outperform LiDAR sensors.

Machine learning based sensor fusion algorithms, such as the one evaluated in this research, are highly compatible with similarly set up systems given similar input data and optimized training parameters as needed. LSTM (Long-Short-Term-Memory) recurrent neural networks (RNN) have shown promising results in similar sensor fusion applications [9], as they have advantages in classifying rapidly updating, and noisy data. In general, sensor fusion is known to increase measurement accuracy and decrease noise while traditional methods involve manually inputted assumptions, and confidence weights that vary over environmental conditions. Given conditional advantages for different sensors in a system and random sensor noise over time, recurrent neural network based fusion algorithms are reasonable to assume as viable to be applied.

Environmental Impact on Sensors

Furthermore, environmental conditions play an impact on the performance of the sensors. For instance, speed of the sound wave released to the environment is variably based on the relative humidity and temperature conditions present in the medium as well as the concentration of CO_2 [10].

LiDAR sensors operation is impacted due to inclement weather such as rain, fog and snow [12]. One of the reasons of why sensors are impacted by weather conditions is due to Mie Scattering. Since the transmission wavelength of the sensors (LiDAR for instance) is close to or smaller to 6mm, the sensor signal is subjected to Mie scattering which produces the back-scattered signal to be disturbed or produce false signals. Another impact from the environment in LiDAR performance is the dependency of the signal based on the color of the targets in the environment. Due to the nature of the visible electromagnetic spectrum, darker colors absorb more infrared energy than bright colors, reducing environmental recognition on targets with darker colors [13]. The effect of Mie Scattering on radar signals decreases the maximum range that a radar sensor can provide under raining conditions. The effect of precipitation in cameras produces degradation and, in quality of the images taken reducing the object recognition of the environment increasing the danger of a potential crash scenario [11].

For this reason, sensor fusion provides a more robust system by allowing the vehicle to not rely on a single sensor reading but on a variety of them. This allows the system to adapt based on the environment following a correct measurement of the environment avoiding out-of-range measurements and noise. More accurately and efficiently interpreting high-speed data from an array of sensors not only can improve the judgment of existing autonomous control systems but also allow the development of new safety features. Currently, the

TABLE 2 Performance summary ADAS sensors [11]

Feature	LiDAR	Radar	Ultrasonic
Technology	Laser beam	Radio wave	Sound Wave
Range (m)	200	250	5
Resolution	Good	Average	Poor
Weather impact	Yes	Yes	Yes
Detects speed	Good	Very Good	Poor
Detects distance	Good	Very Good	Good

FIGURE 3 Sensor Fusion Architecture Schematic

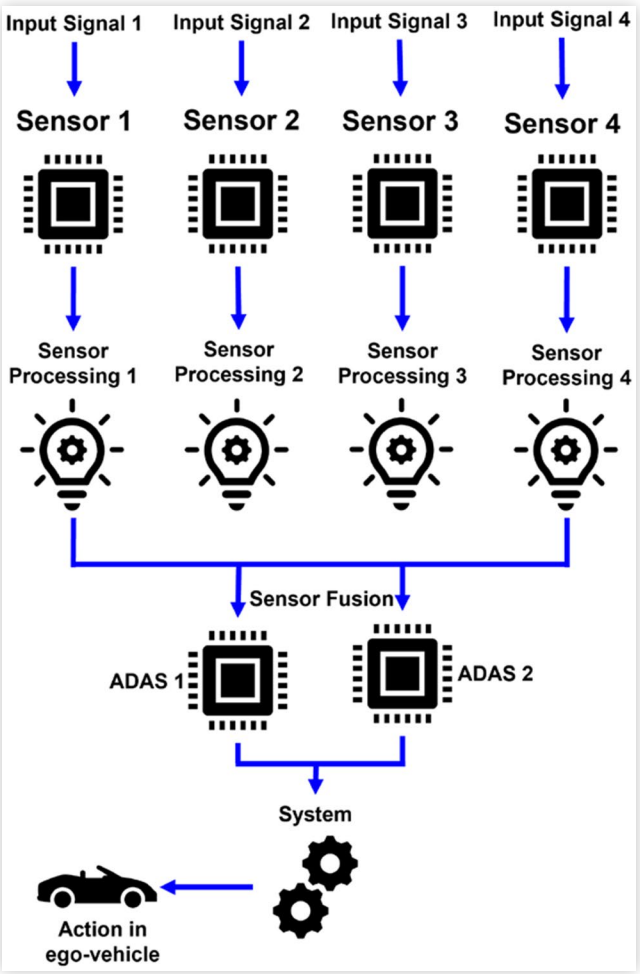

performance of sensor fusion systems is not limited by sensing range or computational power, but rather by the quality and efficiency of their harmony. By varying crucial conditions based on predicted drawbacks of their components, complex sensor fusion systems can be optimized and the nature of their effects analyzed.

Previous Research and Applications

Fusion of thermal and visible light detection sensors using neural networks was studied in [2]. A new Adaptive Soft-Gated Light Perception Fusion (ASG-LPF) as a model for fusion was proposed. The ASG-LPF framework begins with image acquisition using a data-set from KAIST (set of paired visible color and thermal color images). Images are then passed through the pedestrian detection and light perception modules which predict the position of pedestrians and the light illumination of a scene. The main detecting sensor was determined by prediction of driving illumination. During sensor fusion the main detector was chosen utilizing fusion filters and weight fine tuning to adjust confidence scores and then remove redundant and low-scoring results. Authors in [14] created a framework for the integration of simulation and sensor fusion data for the improvement of learning data sets. Data fusion occurs at different levels. The most basic method occurs where raw data from separate sources is combined. At the next level features from each source are combined into a single delineation. This is known as 'feature-level fusion'. It allows for the characterization of patterns by different observed features. Another level above is 'decision level'. In this level of fusion models trained on varied sources make a decision based on the presented data.

To improve object detection by way of data fusion of stereo images and ultrasonic sensors, [15] proposed an algorithm where the ultrasonic sensors were used to locate the nearest object layer of the modified local stereo algorithm. This decreased amount of search layers led to the generation of incorrect responses that were reduced by use of the reduced cross-check method. A median filter was also used to improve accuracy. The authors then demonstrated improved time of detection by use of 'synthesis' images produced in Blender. Detection times were improved by 316 times. To demonstrate improved environmental perception, [16] used a Nomad 200 robot equipped with ultrasonic and laser rangefinders modeled with fuzzy logic. Readings were used by the robot to build a model of its environment then using a reliability test determined if readings were incorrect, getting rid of bad data. This was done by comparing the differences in readings from each sensor within the plane area of the sonar sensors. Significant improvement of environmental modeling was shown with errors present in single sensor type use cases being corrected by use of fusion of the two sensor types.

To classify tree trunks and to help localizing a robotic platform for use in orchards, [17] used cameras and ultrasonic sensors. Trunks were classified by a recognition and classifier algorithm (SVM) which discerned trunks by color recognition. The ultrasonic sensors were used in order to minimize the detection of meaningless data beyond the range of tree trunks in the semi-structured orchard. This helped to decrease measurement error when localizing tree trunks. An average was also applied to minimize detection error. Ultrasonic sensors improved localization as compared to laser detection sensors used in past studies.

ADAS with Sensor Fusion Integration

ADAS systems are based on sensor fusion algorithms where sensors complement each other reducing their limitations and expanding their field of view for an enhanced environment perception. This principle is accomplished by using data synchronization where data originated from different sensor sources is fused and then, is synchronized and applied in ADAS systems. This increments the precision of data as well as the certainty of it. Furthermore, this data is used in different applications within the vehicle (AEB, blind spot detection, ACC, LDW) since these technologies rely on the data from the same sensors but it is processed independently based on the ADAS feature specified.

A sensor fusion architecture process in safety vehicle technologies contains different sets of sensors feeding the system with data. Once this data is compiled, it is processed and synchronized ready to take action in the ADAS features integrated in the vehicle. It is important to process this data in the same order it has been acquired to obtain a time-consistent sensor fusion model as researched in [18].

Active driving assistance systems can be understood as semiautonomous vehicles. However, these type of technologies support the drivers to relieve stress and fatigue for driving long hours or for driving under high traffic conditions. For instance, [19] describes multiple technologies for ADAS systems that include sensor fusion. One of them is Cadillac's Super Cruise, where different highways around the country have been scanned with LiDAR data creating a map of the surroundings for highway recognition and positioning. Furthermore, ACC and LKA is enabled for this feature, allowing hands free driving. The feature works as long as the driver is focused on the road which is monitored with a camera scanning the driver. In this ADAS feature, sensor fusion is integrated by using data coming from different sources of sensors. LiDAR, Radar and camera data is combined together and processed to create a safe hands free driving technology [20]. Pseudo inverse based on point alignment method was used in [21] to calibrate and match the output of radar sensors with cameras to enhance object recognition in autonomous vehicles. Another method for vehicle recognition based on sensor fusion is demonstrated in [22], where the field of view of the radar sensor is coordinated with a camera, achieving vehicle localization based on the rear corner recognition of vehicles on the road.

Methodology

Proposed Vehicle Safety Envelope Principle

The model vehicle safety envelope proposed in this work shows the definition of two zones around the ego vehicle (dense and critical zone), each named to indicate the importance of measurement precision. Each zone was divided into equal intervals (0.05m each) to enhance the precision of obstacles detected within each of the zones in the enclosed area of the envelope. An LSTM machine learning prediction model was trained in order to fuse the signal of the three sensors selected to enhance precision of the vehicle envelope. Furthermore, the data acquired from the sensors in the envelope are displayed in a live data simulation graph, allowing the user to see the data that sensors are acquiring from the environment in a radar schematic. Each zone classification was displayed on these graphs to represent both the critical and non-critical risk of collision regions. The proper distance measurements within such a vehicle safety envelope would allow better environmental awareness for imminent collisions and their avoidance.

FIGURE 4 ADAS Sensors Instrumented in Vehicle Platform.

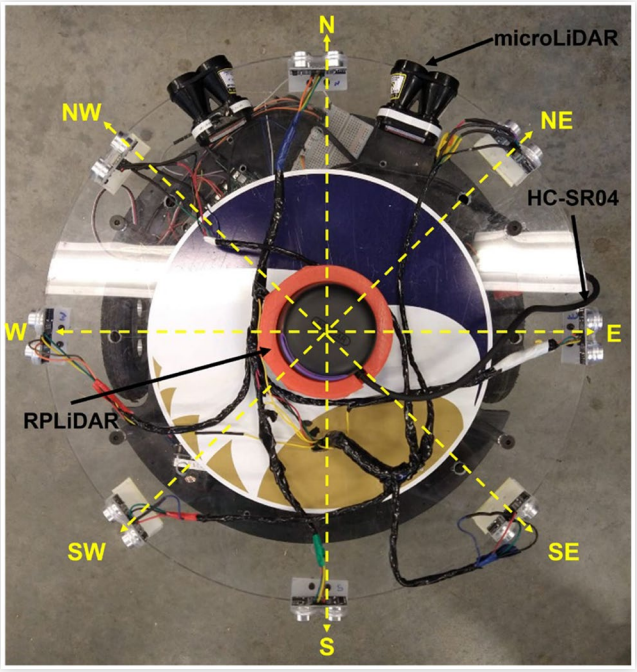

The methodology presented for this experiment includes assembly of ego vehicle, implementation of sensors used in the safety vehicle envelope system, controlled environment with mobile target configuration, vehicle safety sensors data acquisition and LSTM sensor fusion training.

Implementation of Sensors

A set of three different sensors were used to instrument the ego-vehicle. These sensors include: Ultrasonic sensors (HC-SR04), a 2-D LiDAR (RPLiDAR) and a laser rangefinder (SF11-C). These sensors were installed on top of the ego vehicle and distributed in a 360° field of view to cover the cardinal directions. The criteria used to choose the sensors for this project is based on the advantages and disadvantages of each sensor, aiming for a sensor fusion structure that would complement each sensor's performance while also enhancing environmental recognition. For example, the HC-SR04 perform best at a short-range distance. For this reason, this sensor's fundamental purpose is to detect obstacles at a range of 0.05 m to 0.25 m. Alternatively, both the RPLiDAR and SF11-C have higher precision and recording range that allows the recognition of objects at much longer ranges, making these sensors the best fit for detecting objects within the Dense Zone. This combination of sensors creates a fusion of sensor signals with precise obstacle recognition for both short and long range targets.

Controlled Environment using Mobile Target Configuration

The set up used for this work consisted of two controlled environment stations, each with a total area of 0.70 m × 0.535 m. Within each station, a test range was created from 0.00m to 0.50m, divided into intervals of 0.05 m. A flat steady environmental condition chamber was built. Within this chamber, a target was moved to each distance increment and the data coming from each sensor was collected for five hours. Each station was equipped with a set of the three sensors used for the sensor fusion located at the origin position and directed towards the target. Two of these controlled environment stations were created in order to record the data necessary twice for methodology validation purposes and evaluation of the interchangeability of proposed sensor fusion models.

Data Acquisition for Vehicle Sensors

A data acquisition algorithm was created to record extensive amounts of data to feed the machine learning model for LSTM prediction training. Each distance was measured until 378,000 data points were taken. Each sensor was directed at the target object with an equal distance from the origin. This data was taken a total of 10 times, one at each 0.05 m interval, in order to acquire data from all distances necessary for the LSTM training. With each data set having 378,000 data points, a total of 3,780,000 points recorded of all distances.

FIGURE 5 Controlled Environment Used for Sensor Data Acquisition

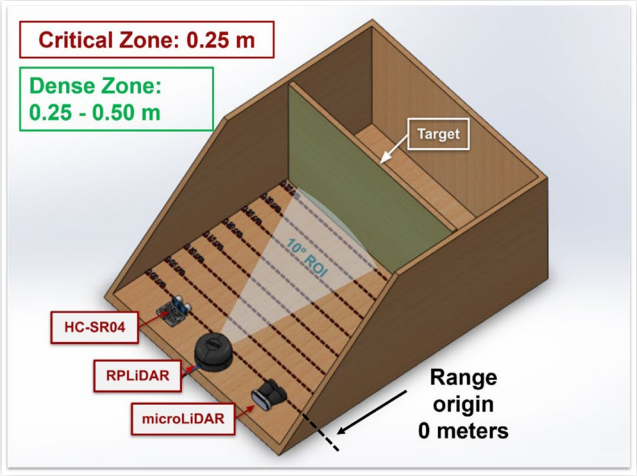

The HC-SR04 required an interface with Arduino in order to record data to MATLAB. The RPLiDAR and SF11-C sensors were connected straight to the serial ports of the computer used for data acquisition. Due to the 360° field of view of the RPLIDAR sensor, it was determined that a region of interest was required to reduce recorded data that did not include the target data points. This ROI was defined to record data points enclosed in a +5° and -5° field of view with respect to the x-z plane shown in Figure 4.

With this reduction of points performed in the ROI, the number of data points was reduced substantially resulting in 11782 data points. These data points were then fed into the LSTM prediction model. Each one of the sensor data matrices fed into the LSTM machine learning model contained RPLiDAR data, ultrasonic sensor, laser rangefinder and time between recorded ROI points.

FIGURE 6 Raw Sensor Measurements Data Points 0.45m ROI

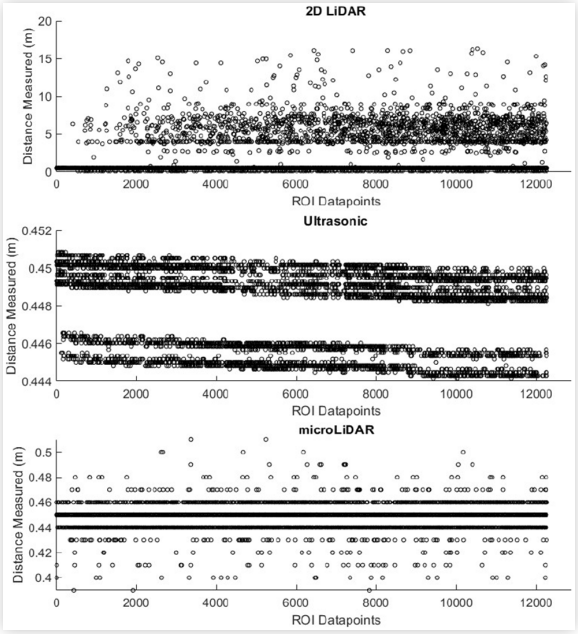

Pre-Training Feature Evaluation

Before developing a machine learning algorithm, the ROI data sets were analyzed to find features of input data relevant to the true distance measured. Given the scope of the project, three inputs are required, the distance measurements of LiDAR, ultrasonic and microlidar sensors. Figure 6 below shows the raw distance measurement distributions of each sensor.

As seen in Figure 6, all sensors have considerable noise which can be mitigated in the fusion process if the network is properly trained. To account for noise, it is essential to train to train the LSTM model with an accurate sense of time for each data point. As seen in Figure 7, the time response between ROI datapoints varies greatly over time. To account for noise and accommodate the inconsistent detection of the ROI by the 2D LiDAR, the time between data points were added as an input for each measurement.

FIGURE 7 Time Response Between Data Points 0.45m ROI

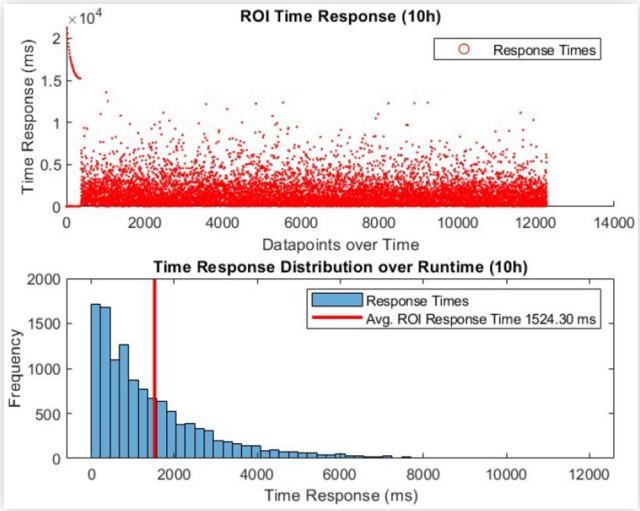

Unlike the ultrasonic and microLiDAR sensor, the 2D LiDAR sensor measures distances in more than one direction. While the ROI was defined in pre-processing as a small region between -5 and 5 degrees (x-z plane) and the distances measured at each ROI angle are insignificant, this is not the case when this model is used in a dynamic setting with all angles measured meaning the angle must be considered in training.

Prediction Model - LSTM

With the ROI data separated, they were respectively split in half: the first half was used for LSTM training and the second half was used to evaluate the trained neural network. This was

done for a fair evaluation of the neural network's performance by testing with data not used in the training process. The sequence-to-sequence regression neural network designed to perform sensor fusion is a double-LSTM deep neural network as seen in Figure 8 below.

FIGURE 8 Diagram of LSTM Network Layers

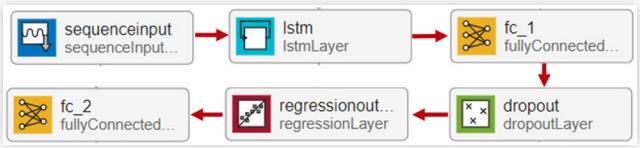

The network consisted of seven layers: an input layer (sequence input), two LSTM layers, two dropout layers, a fully connected layer (fc 1), and a regression layer. The first layer was an input layer of four units, one for each data point recorded from the sensor fusion: the ultrasonic measurement, the microLiDAR measurement, the 2D LiDAR measurement and the time, in milliseconds, since the last measurement. Directly following the input layer, is the first LSTM layer with 125 hidden units. Next is the first dropout layer with a probability of 0.3. After the first dropout layer is the second LSTM layer, again with 125 hidden numbers, followed by the second dropout layer, this time with a probability of 0.2. Finally, there is a fully connected layer with one unit. This final output represents the LSTM Fusion distance.

TABLE 3 Sample Fusion Input Column of Sensor and Time Data

Input	Value
LiDAR Angle (deg)	1
LiDAR Distance (m)	0.5
Ultrasonic Distance (m)	0.5
microLiDAR Distance (m)	0.5
Time Difference From Last ROI (ms)	1300

For both training and testing, the sequence input of the evaluated LSTM sensor fusion algorithm consists of a matrix of x columns (data points measured), and five rows (sensor data). The first row was the angle in degrees at which the LiDAR was facing when the given ROI data point was taken. The second row was the distance in meters of the LiDAR's distance measurement when the ROI was measured. The third row was the distance in meters of the ultrasonic sensor's measurement. The fourth row was the distance in meters of the microLiDAR. For training, the first half of the distance's data point columns of five rows were sequentially fed with a separate row of the repeating true distance measured. To test the trained sensor fusion model, the second half of the data points were each given as an input to the trained network, and for each data column given, an output of a fusion distance was provided.

Results

Machine Learning Based Safety Vehicle Envelope

All machine learning sensor fusion results presented were found using the second half of each distance's data set. This was done as the first half was used for training and the fusion algorithm must be evaluated with data it has not used to perform learning. The results are structured according to the algorithm's evolution: first showing the fusion performance when each distance had a dedicated fusion algorithm and lastly showing the fusion performance when all measured distances had only one fusion algorithm. For the first phase, the dedicated testing data of each measured distance was fed into a corresponding LSTM network, trained for fusion only at the measured distance. For the second phase, all of the same dedicated testing data of all distances were fed into one LSTM neural network able to do fusion at all distances measured.

The critical zone of the vehicle safety envelope was defined at a distance of 0.05 m to 0.25 m. This zone was then divided into five separate intervals each 0.05 m apart. The performance of the LSTM machine learning algorithm resulted in a high precision fusion of signals of the three sensors used in this work.

Figure 10 shows the LSTM performance for the 0.05m distance. The graph shows the performance of fusing the signal of the three sensors up to a point in which the prediction is close to the ground truth distance of 0.05m. At the beginning of the data set, the model takes some time to fuse the signals precisely to the ground truth. Nevertheless, once the tester algorithm is close to 800 data points, the predicted data starts oscillating on the ground truth distance.

As shown in the Figure 9, LSTM performance is shown with the intervals from 0.05m up to 0.50m. Average values of resultant prediction distance for each one of the intervals was calculated. As shown in table 5, standard deviation between the ground truth value and the average LSTM calculated was

FIGURE 9 Individual and compilation LSTM performance. a) shows the performance comparison of the individual based LSTM machine learning model. b) shows the performance comparison of the compiled LSTM machine learning model including all distances for training.

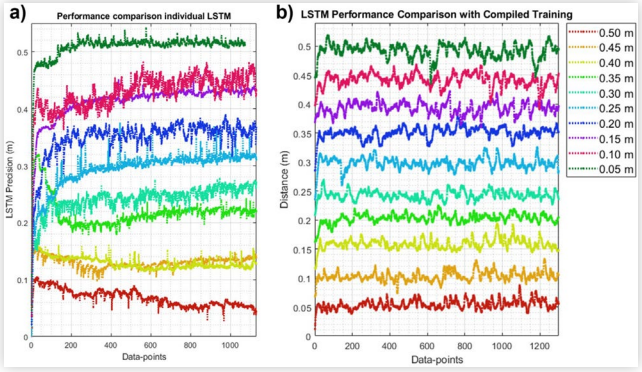

FIGURE 10 Individual LSTM performance 0.05m

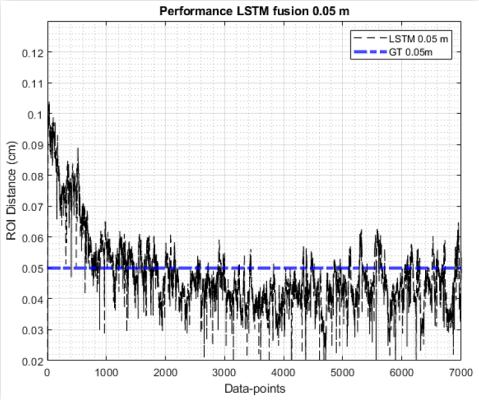

considerably low, resulting in high precision of obstacle distance estimation.

The percentage error calculated for the critical zone had a range between 3.99% and 10.67%. This resultant percentage error represents low error in the study and suggests validation of the use and integration of this LSTM distance estimation model for the vehicle safety envelope.

The dense zone of the vehicle safety envelope was defined at a distance of 0.30 m to 0.50 m. Much like the critical zone, the dense zone was divided into five separate intervals of 0.05 m.

The dense zone performance shows a constant behavior of the LSTM model where the error percentage ranges between 1.07% and 9.34%. The average distances recorded from the LSTM model with respect to the ground truth distances are close to the ground truth reference value. This is reflected on the standard deviation values calculated as well as the percentage error. Data precision is demonstrated on the graphs and shows a successful data fusion model.

TABLE 4 Statistical Analysis of Individually Trained Fusion Algorithms Performance

Ground Truth (m)	Average Fusion (m)	Std. Deviation (m)	% Error
0.05	0.0480	0.0014	3.99
0.10	0.1179	0.0127	9.00
0.15	0.1293	0.0147	5.81
0.20	0.2213	0.0151	10.67
0.25	0.2636	0.0096	5.46
0.30	0.3280	0.0198	9.34
0.35	0.3644	0.0102	4.11
0.40	0.4226	0.0160	5.65
0.45	0.4528	0.0034	1.07
0.50	0.5081	0.0057	1.62

TABLE 5 Statistical Analysis of Compiled Trained Fusion Algorithms Performance

Ground Truth (m)	Average Fusion (m)	Std. Deviation (m)	% Error
0.05	0.0547	0.0081	9.4
0.10	0.1034	0.0086	3.36
0.15	0.1591	0.0091	6.05
0.20	0.2034	0.0083	1.69
0.25	0.2424	0.0080	3.03
0.30	0.2970	0.0010	1.00
0.35	0.3507	0.0010	0.21
0.40	0.3920	0.0115	2.00
0.45	0.4408	0.0117	2.04
0.50	0.4914	0.0114	1.71

FIGURE 11 ADAS Sensors Instrumented in Vehicle Platform

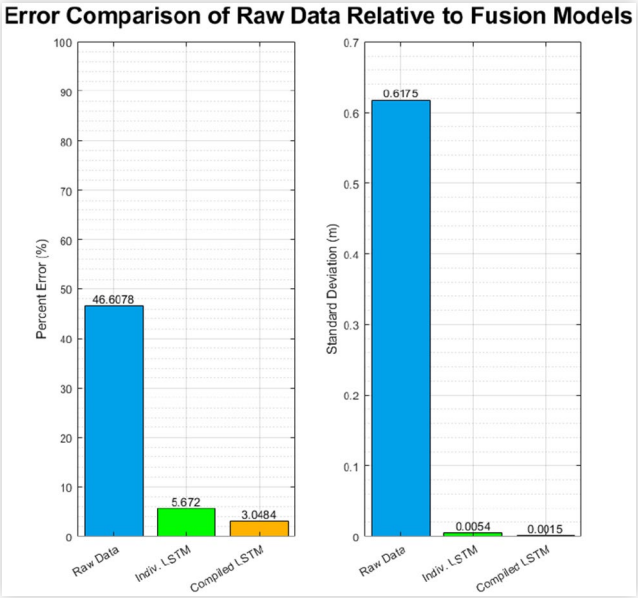

Live Data Simulation

The live data simulation integrated in the ego-vehicle fuses the signal of the three sensors and displays it in a single graph for live environment visualization. This allows the user of the vehicle to be aware of all readings from the sensors in a graphic interface for constant monitoring. Eight different ultrasonic sensors were integrated in the test platform for each cardinal direction, one RPLiDAR was centered in the middle of the vehicle for a 360° view and finally two microLiDARs were assembled for the North East and North West directions.

FIGURE 12 Visual Representation of Safety Zone Distances

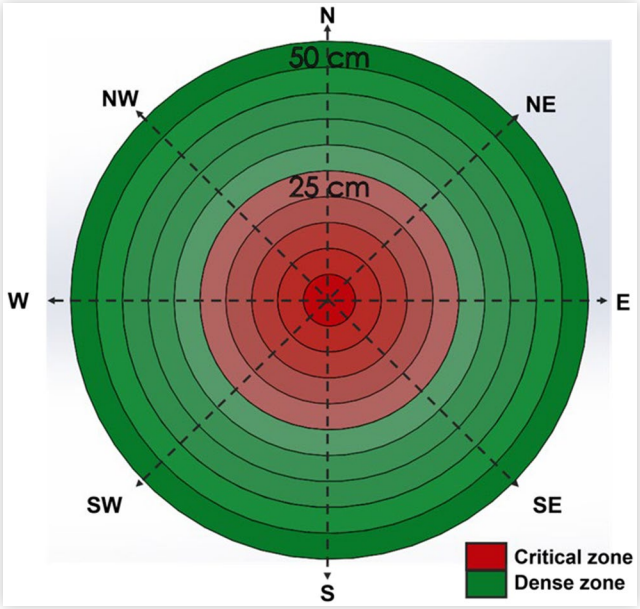

Figure 13 shows the sensor data fused in a radar graph. This data visualization is important to show the performance of the recording of the sensors while validating the data recorded complementing each other. For short ranges, signal acquired from the ultrasonic sensor was more precise and reliable than the LiDAR sensor. For this reason, it was possible to see some discrepancies of data recorded in a close range.

Meanwhile, the LiDAR sensor is very precise for long distance measurements. This is shown on how sensors compensate each other in the LSTM model, where with the combination of the sensor signals, distance recorded is more precise.

FIGURE 13 Visual API used to Represent Live Data - Simulated

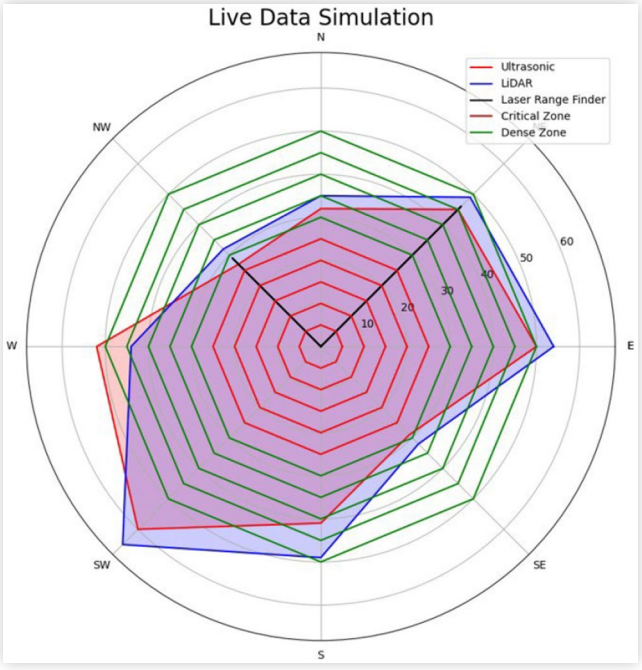

The importance of this visualization is to rely not just on the readings of the sensors graphically but also being able to visualize this data from a spatial perspective. This graph displays the ego vehicle as the origin of the radar simulation. Then all data displayed from all the cardinal directions where the sensors were instrumented in the ego-vehicle.

Conclusion

The LSTM machine learning model used in this project allowed for the fusion of the signals of three different distance sensors (ultrasonic sensors, RPLiDAR and microLiDAR) based on two different physical principles (sound and light) with the aim to enhance the precision of distance recorded for the vehicle safety envelope. The vehicle safety envelope was designed enclosing a max recording distance range of 0.50 m. Within this maximum distance of the envelope, two zones were defined, dense and critical zones, with ranges of 0.25m - 0.50m and 0.05m - 0.25m respectively.

Dense and critical zones were trained using an LSTM model combining the signals of the sensors aiming for high distance estimation precision for enhancing safety in the ego-vehicle. The structure used for training and testing was a sequence input of the LSTM sensor fusion that consisted on a matrix of number of points and five rows of sensor data. The sensor data selected included angles recorded from LiDAR ROI, distance in meters from ROI recorded from LiDAR, distance recorded from ultrasonic sensor, distance recorded from the microLiDAR.

Meanwhile, distance recorded from every sensor was displayed in a radar graph. The output of the machine learning based sensor fusion created a high precision vehicle safety envelope recognizing obstacles moving within the range of the envelope. The results given from the LSTM model were successful, the percentage error for individual and compiled training set up was 5.67% and 3.05% respectively demonstrating a high precision sensor fusion prediction model. On the other hand, standard deviation on individual and compiled LSTM models was 0.0054% and 0.0015%. The lowest percentage error for compiled LSTM model was 0.21% showing a precise distance measurement using the three signals from the distance sensors.

Future Work

With the introduction of the 360° vehicle safety envelope with possible collision risk classification, the static study has been performed with high precision sensor fusion data recording. Precision for recording of distance of obstacles within the range determined is ready for implementation in dynamic scenarios where the ego-vehicle has interaction with targets in motion for tracking and environment monitoring. Further work will include performing corrective steering for crash

avoidance based on the obstacles detected within the safety vehicle envelope and their established safety zones.

References

1. Singh, S., *Critical Reasons for Crashes Investigated in the National Motor Vehicle Crash Causation Survey* (National Highway Traffic Safety Administration, 2015)
2. Li, G., Lai, W., and Qu, X., "Pedestrian Detection Based on Light Perception Fusion of Visible and Thermal Images," *Optics & Laser Technology* 156 (2022): 108466.
3. Greene, D.L., Baker, H.H. JR., and Plotkin, S.E., *Reducing Green-House Gas Emissions from U.S. Transportation*, 2010.
4. Brown, N.E., Rojas, J.F., Goberville, N.A., Alzubi, H. et al., "Development of an Energy Efficient and Cost Effective Autonomous Vehicle Research Platform," *Sensors* 22, no. 16 (2022).
5. Erlien, S.M., Fujita, S., and Gerdes, J.C., "Safe Driving Envelopes for Shared Control of Ground Vehicles," *IFAC Proceedings Volumes* 46, no. 21 (2013): 831-836.
6. Erlien, S.M., Fujita, S., and Gerdes, J.C., "Shared Steering Control Using Safe Envelopes for Obstacle Avoidance and Vehicle Stability," *IEEE Transactions on Intelligent Transportation Systems* 17, no. 2 (2016): 441-451.
7. Griffor, E., Wollman, D., and Greer, C., "Automated Driving System Safety Measurement Part 1: Operating Envelope Specification," 2021.
8. Sakib, S.M.N., "Lidar Technology - an Overview," *IUP Journal of Electrical Electronics Engineering* 15, no. 1 (2022): 36-57.
9. Li, H., Shrestha, A., Heidari, H., Le Kernec, J. et al., "Bi-Lstm Network for Multimodal Continuous Human Activity Recognition and Fall Detection," *IEEE Sensors Journal* 20, no. 3 (2020): 1191-1201.
10. Panda, K.G., Agrawal, D., Nshimiyimana, A., and Hossain, A., "Effects of Environment on Accuracy of Ultrasonic Sensor Operates in Millimetre Range," *Perspectives in Science* 8 (2016): 574-576.
11. Vargas, J., Alsweiss, S., Toker, O., Razdan, R. et al., "An Overview of Autonomous Vehicles Sensors and their Vulnerability to Weather Conditions," *Sensors* 21, no. 16 (2021).
12. Goberville, N., El-Yabroudi, M., Omwanas, M., Rojas, J. et al., "Analysis of Lidar and Camera Data in Real-World Weather Conditions for Autonomous Vehicle Operations," *SAE International Journal of Advances and Current Practices in Mobility* 2, no. 5 (2020): 2428-2434.
13. Sequeira, G.J., Harlapur, B., Ortegon, D.O., Lugner, R., Brand-meier, T., and Soloiu, V., "Investigation of Influence from Variation in Color on Lidar Sensor for Perception of Environment in Autonomous Vehicles," in *2021 International Symposium ELMAR*, 71-76, 2021.
14. Saadallah, A., Finkeldey, F., Buß, J., Morik, K. et al., "Simulation and Sensor Data Fusion for Machine Learning Application," *Advanced Engineering Informatics* 52 (2022): 101600.
15. Gholami, F., Khanmirza, E., and Riahi, M., "Real-Time Obstacle Detection by Stereo Vision and Ultrasonic Data Fusion," *Measurement* 190 (2022): 110718.
16. Fabrizi, E. and Ulivi, G., "Sensor Fusion for a Mobile Robot with Ultrasonic and Laser Rangefinders *," *IFAC Proceedings Volumes* 30, no. 7 (1997): 351-356.
17. Chen, X., Wang, S., Zhang, B., and Luo, L., "Multi-Feature Fusion Tree Trunk Detection and Orchard Mobile Robot Localization Using Camera/Ultrasonic Sensors," *Computers and Electronics in Agriculture* 147 (2018): 91-108.
18. Kaempchen, N., and Dietmayer, K., "Data Synchronization Strategies for Multi-Sensor Fusion," 09, 2022.
19. Monticello, M., "The Road to Self-Driving Cars," *Consumer Reports* 86, no. 2 (2021): 52-57.
20. Cadillac, "Super Cruise: Hands-Free Driving, Cutting Edge Technology," 9/16/2022.
21. Kim, J., Han, D.S., and Senouci, B., "Radar and Vision Sensor Fusion for Object Detection in Autonomous Vehicle Surroundings," in *2018 Tenth International Conference on Ubiquitous and Future Networks (ICUFN)*, 76-78, 2018.
22. Kang, D. and Kum, D., "Camera and Radar Sensor Fusion for Robust Vehicle Localization Via Vehicle Part Localization," *IEEE Access* 8 (2020): 75223-75236.

Contact Information

Valentin Soloiu, Ph.D.
Director of Intelligent Vehicles Laboratory
Georgia Southern University, USA
vsoloiu@georgiasouthern.edu

Acknowledgments

This research was funded by the US Federal government NSF Grant #1950207.The authors appreciate the support from Mr. John William McAfee (ME) for the contribution to this paper.

Definitions, Acronyms, Abbreviations

ADAS - Advanced Driver Assistance Systems

AV - Autonomous Vehicles

LiDAR - Light Detection and Ranging

NHTSA - National Highway Traffic Safety Administration

NMVCCS - National Motor Vehicle Crash Causation Survey

GNSS - Global Navigation Satellite System
IMU - Inertial Measurement Unit
ToF - Time of Flight
LSTM - Long Short-Term Memory
RNN - Recurrent Neural Networks
ASG-LPF - Adaptive Soft-Gated Light Perception Fusion
SVM - Support Vector Machine
AEB - Automatic Emergency Braking
ACC - Adaptive Cruise Control
LDW - Lane Departure Warning
LKA - Lane Keeping Assist
LDW - Lane Departure Warning
ROI - Region of Interest
GT - Ground Truth

ISSN 0148-7191